Optical Gating of Graphene on Photoconductive Fe:$LiNbO_3$

Jon Gorecki,[*,†] Vasilis Apostolopoulos,[‡] Jun-Yu Ou,[†] Sakellaris Mailis,[†] and Nikitas Papasimakis[†]

Optoelectronics Research Centre, University of Southampton, and Department of Physics, University of Southampton

E-mail: j.gorecki@soton.ac.uk

[*]To whom correspondence should be addressed
[†]Optoelectronics Research Centre, University of Southampton
[‡]Department of Physics, University of Southampton

Abstract

We demonstrate experimentally non-volatile, all-optical control of graphene's charge transport properties by virtue of a Fe:$LiNbO_3$ photoconductive substrate. The substrate can register and sustain photo-induced charge distributions which modify locally the electrostatic environment of the graphene monolayer and allow spatial control of graphene resistivity. We present light-induced changes of graphene sheet resistivity as high as $\sim 370\ \Omega/sq$ (~ 2.6 fold increase) under spatially non-uniform light illumination. The light-induced modifications in the sheet resistivity are stable at room temperature but can be reversed by uniform illumination, or thermal annealing (100°C for 4 hours) thus restoring graphene's electrical properties to their initial, pre-illumination values. The process can be subsequently repeated by further spatially non-uniform illumination.

Keywords

graphene, two-dimensional materials, field-effect transistor, photoconductive, lithium niobate

Graphene, demonstrated to be the world's first truly two dimensional monolayer material in 2004 by Novoselov and Geim,[1] has attracted intense research interest owing to its unique electrical and optical properties. Consisting of carbon atoms arranged in a two-dimensional hexagonal lattice, graphene exhibits a linear dispersion for electrons with the density of states vanishing at the Dirac point. This allows to alter significantly graphene's electronic properties by injecting relatively small numbers of charge carriers.[2] In combination with the inherent high values of charge carrier mobility, these properties render graphene an appealing material for applications such as Microelectromechanical Systems (MEMS),[3] flexible touch-screen electrodes,[4,5] chemical sensing,[6,7] membranes,[8] and especially optoelectronic applications,[9] including photodetection.[10] Graphene has been shown to support strongly confined plasmonic excitations in the Terahertz (THz)/infrared spectral (IR) range,[11] which allows the realization of miniaturized tunable devices.[12–14]

The charge transport properties of graphene are typically controlled through chemical doping,[15] by electrostatic gating[1] or by structuring. In the latter case, for example it is possible to create a bandgap in graphene nanoribbons by patterning or unzipping of carbon nanotubes;[16–18] or by combination with other 2D lattices[19] such as hexagonal boron nitride (hBN),[20] and transition metal dichalcogenides (TMD's).[21,22] In the case of electrostatic gating, a field-effect transistor (FET) configuration is usually employed, where graphene is placed on an Si/SiO_2 substrate acting as an insulated electrical backgate; the current transmitted through the device can then be altered by applying a gate voltage, which regulates the number of available charge carriers into graphene thus modifying the sheet resistivity. However, such doping mechanisms require additional processing steps and/or do not provide substantial control over the spatial distribution of charge carriers. To this end, a number of light-assisted approaches have been put forward including photochemical effects,[23–25] where irradiation leads to exchange of dopants between the atmosphere and graphene, and photo-oxidation of organic layers resulting in non-reversible charge transfer.[26] In addition, it has been shown that combining light illumination with an electrostatic gate can lead to

charge exchange between graphene and the substrate.[27–29] Finally, depositing graphene on substrates with ferroelectric and pyroelectric properties allows to control either through local electrostatic fields[30] or laser heating,[31] respectively. Here we present an approach towards spatially resolved control of the charge transport properties of monolayer graphene that is both reversible and non-volatile allowing for electrostatic charge distributions to be written or erased in an all-optical fashion.

Our approach is based on a Fe doped lithium niobate (Fe:$LiNbO_3$) substrate, an electro-optic photoconductor that has been studied extensively in the past as a holographic storage medium.[32] $LiNbO_3$, is an artificial dielectric crystal, which has found a multitude of uses in optoelectronics due to its combination of ferroelectric, pyroelectric, piezoelectric, electro-optic (Pockels), photovoltaic, and photo-elastic effects.[33] $LiNbO_3$ suffers from a photo-damage effect;[34] Fe ion impurities in the crystal act as photo-excited charge centres, supplying electrons to the conduction band, which are free to migrate in the lattice. Depending on their valance state these impurities can act as donors or acceptors, thus by non-uniform illumination of the substrate photoexcited electrons diffuse away from the irradiated area to dark regions where they become trapped in acceptor Fe^{+3} sites creating a non-uniform charge distribution which is stable at room temperature over long periods of time (years).[35] This ability to store photo-induced charge distributions locally, combined with the electro-optic effect which is inherent to the material enabled the use of Fe:$LiNbO_3$ for the non volatile recording of holograms,[32] optoelectronic tweezers for manipulating nano-objects,[36] and optically aligned liquid crystal devices.[37] Here, we employ the photorefractive properties of Fe:$LiNbO_3$ to define the local electrostatic environment at the substrate surface using light. The schematic in Figure 1(a) illustrates the optical doping mechanism; non-uniform illumination of the substrate causes electron migration away from illuminated regions creating a non-uniform surface charge distribution. This effect is capable of producing non-volatile charge distributions of arbitrary shape, which can however be erased by uniform illumination or thermal annealing, that redistributes equally the separated charge carriers. A graphene

sheet on the surface of the substrate will experience an injection of charge carriers in response to the electrostatic environment of the Fe:$LiNbO_3$; as the charge carriers are injected the Fermi level of the graphene is significantly altered, modifying its electrical properties. Here, we demonstrate a non-volatile $\sim$ x2.6 increase of the sheet resistivity of chemical vapour deposition (CVD) grown monolayer graphene, which is subjected to the electric field of the substrate's local charge distributions. We show that the changes in the electrical properties of graphene are reversed by thermal annealing, and in fact literature suggests this behaviour of Fe:$LiNbO_3$ can be repeated indefinitely.[32] We propose that the optical doping mechanism demonstrated here will enhance the potential of graphene for remote sensing applications, rewritable electrical interconnects, and will allow the realization of plasmonic devices defined by structured illumination, removing the need for lithographic patterning of graphene. Moreover, the doping method demonstrated here is expected to be compatible with a wide range of TMD's and other 2D materials and hence will be of interest for numerous electronics and optoelectronics applications, including light emission and detection, optically controlled FETs, and sensing.[38–41]

Results and discussion

For the purpose of our investigation we fabricated devices that consist of a uniform monolayer of CVD graphene, transferred to one of the polar surfaces (-z) of Fe:$LiNbO_3$ substrates. An array of gold metallic electrode pairs with varying spacing between them (see Methods) was fabricated on the graphene film. An optical microscopy image of the electrode arrangement is shown in the inset of Figure 1(b). Raman spectroscopy was used to characterize the graphene layer. The ($\sim$2:1) 2D/G peak ratio, observed in a Raman spectrum (Figure 1(b)), which has been obtained in a position between the electrodes, indicates the presence of a single graphene monolayer.

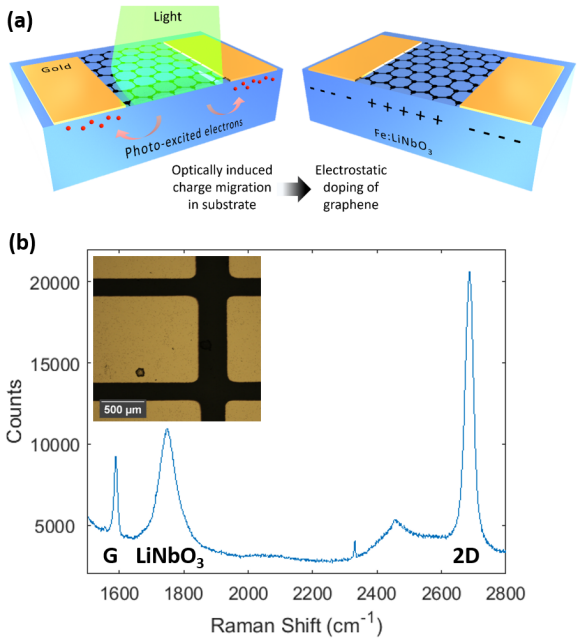

Figure 1: (a) Schematic illustration of the electrostatic environment in a graphene/ $Fe:LiNbO_3$ composite under illumination. In the substrate, electrons photoexcited from Fe^{+2} centres to the conduction band are free to migrate in the lattice until being trapped by Fe^{+3} centres in the dark regions. This results in a non-uniform charge distribution in the substrate, and subsequently to a spatially inhomogeneous electrostatic environment for the graphene layer, which in turn leads to inhomogeneous doping of the graphene layer. (b) Raman spectrum of graphene on a $Fe:LiNbO_3$ substrate exhibiting the graphene G peak at $\sim$1580 cm^{-1} corresponding to an in-plane vibrational mode, the 2D peak at $\sim$2700 cm^{-1} attributed to an overtone of the defect activated D peak (not pictured here), and the 2E lithium niobate peak at $\sim$1750 cm^{-1}. Inset: Reflection mode optical microscopy image of the sample surface with deposited metalic electrodes. The dark regions between the electrodes correspond to the exposed parts of the (non-reflecting) graphene layer.

To illustrate the optical gating of graphene on $Fe:LiNbO_3$ the device was illuminated intermittently with alternating "bright" and "dark" periods (corresponding to "on" and "off" intervals in Figure 2, respectively). The resistance was measured at the end of each "bright" period and was monitored continuously during "dark" periods. The graphene-on-$Fe:LiNbO_3$ devices were illuminated uniformly using a low intensity broadband light source (1 mW/cm^2). However, the metallic electrodes are opaque, which lead to a non-uniform irradiation of the $Fe:LiNbO_3$ substrate, where the area between electrodes was irradiated while the area under the electrodes remained dark. Current was not measured during illumination

periods to avoid the applied potential voltage difference from influencing the migration of photoexcited electrons in the substrate (see Figure 2). During the measurement, a voltage of 0.1 V was applied across the electrodes and the current was recorded over a 300 s period while the device was kept in a light-proof box. The shaded areas of the graph correspond to the "bright" irradiation periods, while the clear sections correspond to "dark" periods. The graph shows that the resistance increases after each illumination period, while eventually, the effect reaches saturation with additional illumination producing negligible change in the resistance as the photoelectron donor sites in Fe:$LiNbO_3$ are being depleted. Over the "dark" periods we observe negligible resistance changes ($< 1\%$ or $2\ \Omega$). After saturation the device is thermally annealed in a convection oven at 100°C for four hours to reset it to its initial state.

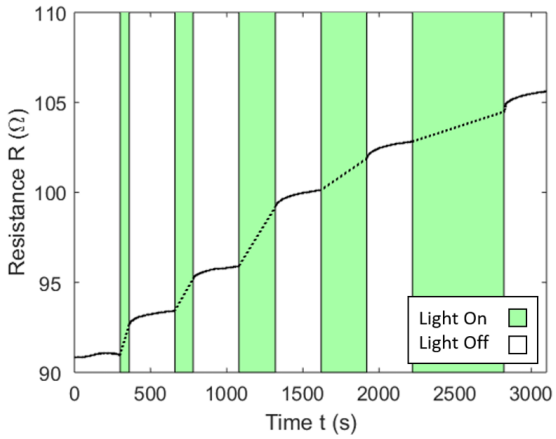

Figure 2: Light-induced changes in the charge transport properties of graphene on Fe:$LiNbO_3$. The sample is intermittently illuminated by white light source with illumination periods of varying duration (shaded regions) being interrupted by 300 sec (non-shaded regions) periods over which the device is stored in the dark. Measurements are obtained only during the latter periods, when the sample is not illuminated (solid black lines). Dashed lines over the illumination periods serve as a guide to the eye.

The observed light-induced resistance changes can be associated to changes in the graphene layer, but also to changes in the contact resistance between the electrode pads and the measurement probe tips. To evaluate the effect of illumination on the graphene resistivity and decouple this from the contact resistance, we employed the transmission line method

(TLM),[42–44] where measurements are taken between electrodes with varying inter-electrode spacing (see Methods). The measured resistance is plotted against the inter-electrode spacing and a straight line is fitted to the data, as shown in Figure 3(a). The slope of each line is used to calculate the resistivity of graphene while the intercept with the vertical axis corresponds to the contact resistance. The TLM measurements were performed in the dark following irradiation steps. Successive irradiation/measurement steps were taken to generate a family of lines, as shown in Figure 3(a), each corresponding to a specific irradiation fluence. The graph shows that with each successive illumination period the gradient of the line is increased, which suggests an increase of graphene resistivity, while the vertical axis intercept is close to the zero point for each fitted line suggesting the contact resistance is small and unchanged by illumination. The average contact resistance is determined to be 1.7 Ω. Thermal annealing of the device (100°C for four hours) resets the device to its initial state and the resistivity measurement sequence can be performed again. We repeated the illumination/annealing cycle three times.

The resistivity change as a function of the illumination fluence is shown in the plot of Figure 3(b). The sheet resistivity values in Figure 3 were calculated from the slope of the linear fits, shown in Figure 3(a) where the standard error of the linear fitting is used to calculate the errors in resistivity values. Data from all three cycles showed similar behaviour and each time resistivity returned to initial pre-illumination values after annealing (see Supporting Information Figure S1 where three individual cycles are shown). Average resistivity of the three illumination cycles is taken for each fluence dose and the errors propagated forward as shown by the error bars in Figure 3(b). The resistivity, ρ follows an exponential increase as a function of illumination fluence, F, which can be fitted by $\rho = a \cdot (1 - exp^{(-F/F_0)}) + c$, where $a = 373\ \Omega/sq$, $F_0 = 6318$ mJ/cm^2, and $c = 231\ \Omega/sq$. This dependence suggests that the effect saturates to a resistivity value of 604 Ω/sq reaching e^{-1} of saturation value at a fluence of 6318 mJ/cm^2 ($\sim$ 2.6 fold increase from initial pre-illumination values). The secondary vertical axis, to the right, in the plot of

Figure 3(b) provides the corresponding values for charge carrier density calculated from the measured resistivity values, electron charge, and using a mobility value of 3760 $cm^2V^{-1}s^{-1}$ as characterised by the supplier of the graphene monolayer. The graph indicates that the carrier density decreases by a factor of ∼3 (corresponding to a modulation of carrier density ∼ 5.5 x10^{12} cm^{-2}) with increasing illumination. A control device consisting of graphene on an Si/SiO_2 substrate with an identical (to the Fe:$LiNbO_3$ sample) electrode array was used to confirm that the changes in graphene resistivity are substrate-specific (see Supporting Information Figure S3), as negligible increase of the resistivity was observed in the control sample as a function of irradiating fluence.

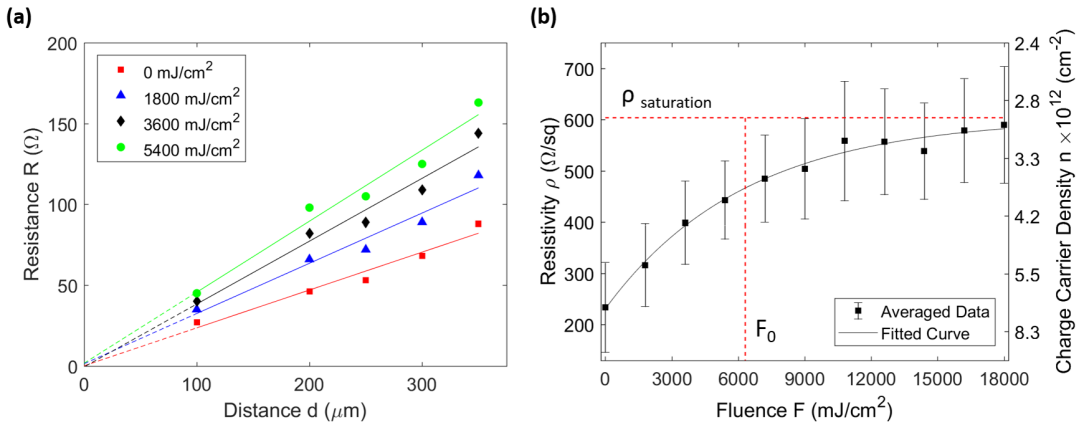

Figure 3: (a) Resistance measured across electrode pairs with varying inter-electrode distance d, for four different values of irradiation fluence. Red squares: non illuminated; blue triangles: 1800 mJ/cm^2; black diamonds: 3600 mJ/cm^2; green circles: 5400 mJ/cm^2. Error bars are omitted because the standard error was four orders of magnitude smaller than the resistance. The straight lines in the plot correspond to linear regression fits. The slope of the lines is used to calculate the sheet resistivity while the vertical axis intercept corresponds to two times the contact resistance. Standard error of the gradient is used to quantify the error in the calculated resistivity value. (b) Graphene sheet resistvity is measured *via* the TLM method as a function of illumination fluence for three independent illumination cycles. Each illumination cycle provides the device with a fluence dose of 18000 mJ/cm^2 at which point further changes in resistivity are negligible. The sample is then reset *via* the thermal annealing process. The average resistivities of the three cycles are plotted against fluence showing an inverse exponential trend. An inverse exponential curve is fitted *via* a regression method revealing the effect saturates at a final resistivity of 603 Ω/sq, reaching e^{-1} of saturation value after a fluence dose of 6318 mJ/cm^2. Errors in resistivty at each fluence value are calculated using the standard error of fitted gradient as illustrated in Figure 3(a) for each illumination cycle and propagated forward to account for averaging between the three illumination cycles.

The experimental errors in resistivity values as plotted in Figure 3(b) are due in part to the TLM method which combines measurements across different pairs of electrodes in different areas of the sample, and therefore assumes identical contact resistance across the whole array of contacts and a uniform graphene sheet resistivity. However, we expect that both factors are subjected to spatial variation across the substrate, especially with polycrystalline CVD graphene. Furthermore the deposition of electrodes and electrical probing can be detrimental to the graphene layer. Literature suggests accurate measurements of graphene sheet resistivity and charge carrier mobility can be obtained *via* terahertz time do-

main spectroscopy,[45] the process is non-contact and therefore non-destructive to the sample, furthermore the electrical properties are averaged over a large area defined by the THz beam focal spot which may reduce errors caused by local variation in the properties of graphene.

The observed change in the resistance as a function of nonuniform illumination is attributed to photo-excited electrons in Fe:$LiNbO_3$, which diffuse and become trapped in the dark, non-illuminated, regions (see schematic illustation of Figure 1(a)). This charge migration effect is well documented in Fe:$LiNbO_3$ and can produce space charge distributions that are stable in the dark for long periods of time (years).[35] The response time of charge migration is a function of illumination intensity[46] and can reach sub-ps time scales under pulsed illumination.[47,48] Furthermore, the charge migration effect can create charge distributions of sub-micron dimensions.[35] In particular, as we illuminate the Fe:$LiNbO_3$ crystal we are moving electrons away from the illuminated area and under the electrodes where they become trapped. When the illumination stops this process creates a positive region underneath graphene, which due to its metallic behaviour draws electrons from the electrodes. Because CVD graphene generally exhibits residual hole doping due to the fabrication process[49,50] the injection of electrons due to the illumination will result in a net decrease in charge carrier density and therefore the resistivity is expected to increase with increasing fluence. Assuming the graphene sheet follows a typical behaviour where resistivity reaches a maximal value when charge carrier concentration is zero and decreases as carriers are injected[1] then starting with hole-doped graphene and a sufficiently strong optical doping effect it may be possible to pass over the point of maximum resistivity and therefore begin to decrease the resistivity. The experimental results presented here suggest the optical doping method was not of sufficient strength to shift the graphene entirely from the hole to electron doped region. Practically this may be achieved by the use of an electrical top-gate as an additional method to control the charge carrier density of the device and bring the graphene sheet closer to its charge neutrality point. A top-gate could also be used to bring the graphene to the point of maximum rate of change of resistivity with respect to charge carrier concentration

thereby allowing the optical gating effect on resistivity to exhibit maximum responsivity. The photorefractive sensitivity of Fe:$LiNbO_3$ increases in blue and green regions of the visible spectrum so it is reasonable to assume that if repeated with blue laser irradiation the experiment would achieve lower F_0 values than with broadband white light. Furthermore, the response time of the effect could be reduced by increasing the intensity of the irradiation, *i.e.* using a pulsed source.

The optical method to locally control the graphene doping that is introduced in this work can be readily extended to the control of graphene plasmons. Indeed, our results indicate that illumination can be employed to change the charge carrier concentration of graphene by a factor of 5.5×10^{12} cm^{-2}, which in the absence of intrinsic doping corresponds to a change in the graphene Fermi level of 0.3 eV. Such effects are sufficient to practically switch 'on' and 'off' plasmonic excitations in graphene microstructures over the microwave and THz spectral ranges.[11,51] Moreover, the optical control of the graphene spatial doping profile could allow the definition of graphene plasmonic resonators simply through non-uniform illumination of continuous graphene layers, aleviating thus the requirement for patterning.

We propose that the optical doping mechanism presented here is not limited to application with only graphene, and would be a versatile tool for investigating doping effects in a wide range of emerging 2D materials. Since the initial identification of graphene by Geim and Novoselov the study of 2D materials has grown rapidly into its own field,[52,53] yielding materials with unique properties especially of interest in optoelectronics[54] such as molybdenum disulphide,[55] silicene,[56] and black phosphorus,[57] where a primary motivation for moving to 2D materials beyond graphene is to find materials which exhibit a band gap while still maintaining high values of charge carrier mobility. We expect that our approach will enable sensing applications, rewritable electrical interconnects, and the possibility of reconfigurable plasmonic structures defined by structured illumination.

Conclusions

We have demonstrated non-volatile control of graphene electrical resistivity by virtue of optically driven charge redistribution in iron doped lithium niobate. Graphene on Fe:$LiNbO_3$ was illuminated *via* a broadband white light source achieving a maximum increase in resistivity of ∼370 Ω/sq (∼ 2.6 fold increase) while a control sample of graphene on Si/SiO_2 showed a negligible change in electrical properties after illumination. For graphene on Fe:$LiNbO_3$ we calculated that the charge migration within the substrate can induce charge carrier density modulation on the order of $5.5 \cdot 10^{12}/cm^2$ in the graphene sheet. We have conducted our experiments using broadband white light illumination however the writing speed could be improved using blue or green laser light. The ability to optically control the electrical resistivity of graphene in a spatially resolved, non-volatile, reversible manner will enable the investigation of the electronic properties of graphene and other emerging 2D materials.

Methods

Fabrication Monolayer CVD graphene grown on a copper substrate (obtained commercially from Graphenea) was transferred *via* a sacrificial polymer layer onto z cut Fe:$LiNbO_3$ (0.1 weight %). Metallic electrodes were created *via* thermal resistance evaporation of a Cr/Au layer (5/100 nm) with a shadow mask to partially obscure sections of the substrate to create an array of electrode pads. The metallic electrodes were patterned with a varying inter-electrode distance as required by TLM to decouple the contact and sheet resistivities. A similar procedure was followed for the fabrication of a control sample consisting of a graphene monolayer deposited on Si/SiO_2substrate.

Raman characterization Raman spectroscopy is used to characterise the graphene layer after deposition onto the substrate, using a 632 nm laser source to probe the graphene with a 50x objective lens. The Raman spectrum is shown in Figure 1(b) where the high ratio of heights of the 2D:G peak is a characteristic sign of monolayer graphene.[58] The broad

peak centred around 1750 cm^{-1} is due to luminescence of the Fe:$LiNbO_3$ substrate.

Electrical characterization An Agilent 4155c electrical parameter analyser is used in a two probe configuration to pass a voltage (sweeping from -0.1V to +0.1V in 200 steps) while measuring the current passing through the circuit. The transition line method (TLM) is used to determine sheet resistivity; the method requires an array of electrodes with varying inter-electrode spacing and each assumed to have identical contact resistance. By measuring resistance across a pair of electrodes the total resistance is the sum of two contact resistances and a graphene resistance equal to the sheet resistivity multiplied by electrode width divided by electrode gap. By plotting the total resistance against electrode gap the sheet and contact resistances can be decoupled, where contact resistance is half the value of the Y axis intercept and sheet resistivity is the gradient multiplied by channel width divided by electrode length. A linear regression analysis is used (disregarding any clear outliers) to calculate the line of best fit; the standard error of the gradient is used as an estimate of the error in the sheet resistivity. All measurements are performed in a cleanroom environment to ensure stable control over temperature and humidity conditions. A broadband white light source is used for illumination of the substrate, delivering a power of 1 mW/cm^2 as measured at the surface of the sample, in the wavelength range 400 - 800 nm.

Thermal annealing After illumination devices are thermally annealed in a convection oven (100°C for 4 hours) to restore the Fe:$LiNbO_3$ substrate to a state of uniform charge distribution.

Acknowledgements

The authors thank F. Javier Garcia de Abajo for stimulating discussions. We acknowledge financial support from the UK's Engineering and Physical Sciences Council through the Teranet network (grant EP/M00306X/1). All data supporting this study are openly available from the University of Southampton repository at https://doi.org/10.5258/SOTON/D0521.

Supporting Information Available

Sheet resistivity measurements for three independent illumination cycles, contact resistance characterisation, and control device measurements. This material is available free of charge *via* the internet at http://pubs.acs.org.

References

1. Novoselov, K.; Geim, A.; Morozov, S.; Jiang, D.; Zhang, Y.; Dubonos, S.; Grigorieva, I.; Firsov, A. Electric Field Effect in Atomically Thin Carbon Films. *Science* **2004**, *306*, 666–669.

2. Castro Neto, A. H.; Guinea, F.; Peres, N. M. R.; Novoselov, K. S.; Geim, A. K. The Electronic Properties of Graphene. *Rev. Mod. Phys.* **2009**, *81*, 109–162.

3. Zang, X.; Zhou, Q.; Chang, J.; Liu, Y.; Lin, L. Graphene and Carbon Nanotube (CNT) in MEMS/NEMS Applications. *Microelectron. Eng.* **2015**, *132*, 192–206.

4. Huang, X.; Zeng, Z.; Fan, Z.; Liu, J.; Zhang, H. Graphene-Based Electrodes. *Adv. Mater.* **2012**, *24*, 5979–6004.

5. Bae, S.; Kim, H.; Lee, Y.; Xu, X.; Park, J.-S.; Zheng, Y.; Balakrishnan, J.; Lei, T.; Kim, H. R.; Song, Y. I.; Kim, Y.-J.; Kim, K. S.; Ozyilmaz, B.; Ahn, J.-H.; Hong, B. H.; Iijima, S. Roll-to-Roll Production of 30-Inch Graphene Films for Transparent Electrodes. *Nat. Nanotechnol.* **2010**, *5*, 574–578.

6. Schedin, F.; Geim, A. K.; Morozov, S. V.; Hill, E. W.; Blake, P.; Katsnelson, M. I.; Novoselov, K. S. Detection of Individual Gas Molecules Adsorbed on Graphene. *Nat. Mater.* **2007**, *6*, 652–655.

7. Shao, Y.; Wang, J.; Wu, H.; Liu, J.; Aksay, I. A.; Lin, Y. Graphene Based Electrochemical Sensors and Biosensors: A Review. *Electroanalysis* **2010**, *22*, 1027–1036.

8. Liu, G.; Jin, W.; Xu, N. Graphene-Based Membranes. *Chem. Soc. Rev.* **2015**, *44*, 5016–5030.

9. Bonaccorso, F.; Sun, Z.; Hasan, T.; Ferrari, A. C. Graphene Photonics and Optoelectronics. *Nat. Photonics* **2010**, *4*, 611–622.

10. Liu, C.-H.; Chang, Y.-C.; Norris, T. B.; Zhong, Z. Graphene Photodetectors with Ultra-Broadband and High Responsivity at Room Temperature. *Nat. Nanotechnol.* **2014**, *9*, 273–278.

11. Jablan, M.; Buljan, H.; Soljacic, M. Plasmonics in Graphene at Infrared Frequencies. *Phys. Rev. B* **2009**, *80*.

12. Grigorenko, A. N.; Polini, M.; Novoselov, K. S. Graphene Plasmonics. *Nat. Photonics* **2012**, *6*, 749–758.

13. Fei, Z.; Rodin, A. S.; Andreev, G. O.; Bao, W.; McLeod, A. S.; Wagner, M.; Zhang, L. M.; Zhao, Z.; Thiemens, M.; Dominguez, G.; Fogler, M. M.; Castro Neto, A. H.; Lau, C. N.; Keilmann, F.; Basov, D. N. Gate-Tuning of Graphene Plasmons Revealed by Infrared Nano-Imaging. *Nature* **2012**, *487*, 82–85.

14. Chen, J.; Badioli, M.; Alonso-Gonzalez, P.; Thongrattanasiri, S.; Huth, F.; Osmond, J.; Spasenovic, M.; Centeno, A.; Pesquera, A.; Godignon, P.; Zurutuza Elorza, A.; Camara, N.; Javier Garcia de Abajo, F.; Hillenbrand, R.; Koppens, F. H. L. Optical Nano-Imaging of Gate-Tunable Graphene Plasmons. *Nature* **2012**, *487*, 77–81.

15. Wang, X.; Li, X.; Zhang, L.; Yoon, Y.; Weber, P. K.; Wang, H.; Guo, J.; Dai, H. N-Doping of Graphene Through Electrothermal Reactions with Ammonia. *Science* **2009**, *324*, 768–771.

16. Han, M. Y.; Oezyilmaz, B.; Zhang, Y.; Kim, P. Energy Band-Gap Engineering of Graphene Nanoribbons. *Phys. Rev. Lett.* **2007**, *98*.

17. Son, Y.-W.; Cohen, M. L.; Louie, S. G. Energy Gaps in Graphene Nanoribbons. *Phys. Rev. Lett.* **2006**, *97*.

18. Kosynkin, D. V.; Higginbotham, A. L.; Sinitskii, A.; Lomeda, J. R.; Dimiev, A.;

Price, B. K.; Tour, J. M. Longitudinal Unzipping of Carbon Nanotubes to form Graphene Nanoribbons. *Nature* **2009**, *458*, 872–876.

19. Das Sarma, S.; Adam, S.; Hwang, E. H.; Rossi, E. Electronic Transport in Two-Dimensional Graphene. *Rev. Mod. Phys.* **2011**, *83*, 407–470.

20. Dean, C. R.; Young, A. F.; Meric, I.; Lee, C.; Wang, L.; Sorgenfrei, S.; Watanabe, K.; Taniguchi, T.; Kim, P.; Shepard, K. L.; Hone, J. Boron Nitride Substrates for High-Quality Graphene Electronics. *Nat. Nanotechnol.* **2010**, *5*, 722–726.

21. Britnell, L.; Ribeiro, R. M.; Eckmann, A.; Jalil, R.; Belle, B. D.; Mishchenko, A.; Kim, Y. J.; Gorbachev, R. V.; Georgiou, T.; Morozov, S. V.; Grigorenko, A. N.; Geim, A. K.; Casiraghi, C.; Castro Neto, A. H.; Novoselov, K. S. Strong Light-Matter Interactions in Heterostructures of Atomically Thin Films. *Science* **2013**, *340*, 1311–1314.

22. Geim, A. K.; Grigorieva, I. V. Van der Waals Heterostructures. *Nature* **2013**, *499*, 419–425.

23. Iqbal, M. Z.; Iqbal, M. W.; Khan, M. F.; Eom, J. Ultraviolet-Light-Driven Doping Modulation in Chemical Vapor Deposition Grown Graphene. *Phys. Chem. Chem. Phys.* **2015**, *17*, 20551–20556.

24. Wang, H. I.; Braatz, M.-L.; Richter, N.; Tielrooij, K.-J.; Mics, Z.; Lu, H.; Weber, N.-E.; Muellen, K.; Turchinovich, D.; Klaeui, M.; Bonn, M. Reversible Photochemical Control of Doping Levels in Supported Graphene. *J. Phys. Chem. C* **2017**, *121*, 4083–4091.

25. Tiberj, A.; Rubio-Roy, M.; Paillet, M.; Huntzinger, J. R.; Landois, P.; Mikolasek, M.; Contreras, S.; Sauvajol, J. L.; Dujardin, E.; Zahab, A. A. Reversible Optical Doping of Graphene. *Sci. Rep.* **2013**, *3*.

26. Seo, B. H.; Youn, J.; Shim, M. Direct Laser Writing of Air-Stable p-n Junctions in Graphene. *ACS Nano* **2014**, *8*, 8831–8836.

27. Wang, X.-J.; Zou, L.; Li, D.; Zhang, Q.; Wang, F.; Zhang, Z. Photo-Induced Doping in Graphene/Silicon Heterostructures. *J. Phys. Chem. C* **2015**, *119*, 1061–1066.

28. Ho, P.-H.; Chen, C.-H.; Shih, F.-Y.; Chang, Y.-R.; Li, S.-S.; Wang, W.-H.; Shih, M.-C.; Chen, W.-T.; Chiu, Y.-P.; Li, M.-K.; Shih, Y.-S.; Chen, C.-W. Precisely Controlled Ultrastrong Photoinduced Doping at Graphene-Heterostructures Assisted by Trap-State-Mediated Charge Transfer. *Adv. Mater.* **2015**, *27*, 7809–7815.

29. Jun, L.; Velasco, J., Jr.; Huang, E.; Kahn, S.; Nosiglia, C.; Tsai, H.-Z.; Yang, W.; Taniguchi, T.; Watanabe, K.; Zhang, Y.; Zhang, G.; Crommie, M.; Zettl, A.; Wang, F. Photoinduced Doping in Heterostructures of Graphene and Boron Nitride. *Nat. Nanotechnol.* **2014**, *9*, 348–352.

30. Yusuf, M. H.; Gura, A.; Du, X.; Dawber, M. Local Control of the Resistivity of Graphene Through Mechanically Induced Switching of a Ferroelectric Superlattice. *2D Mater.* **2017**, *4*.

31. Gopalan, K. K.; Janner, D.; Nanot, S.; Parret, R.; Lundeberg, M. B.; Koppens, F. H. L.; Pruneri, V. Mid-Infrared Pyroresistive Graphene Detector on $LiNbO_3$. *Adv. Opt. Mater.* **2017**, *5*.

32. Buse, K.; Adibi, A.; Psaltis, D. Non-Volatile Holographic Storage in Doubly Doped Lithium Niobate Crystals. *Nature* **1998**, *393*, 665–668.

33. Weis, R. S.; Gaylord, T. K. Lithium-Niobate - Summary of Physical Properties and Crystal Structure. *Appl. Phys. A* **1985**, *37*, 191–203.

34. Buse, K.; Imbrock, J.; Kratzig, E.; Peithmann, K. In *Photorefractive Materials and Their*

Applications 2: Applications; Gunter, P., Huignard, J., Eds.; Springer: New York, 2007; pp 83–86.

35. Arizmendi, L.; Lopez-Barbera, F. J. Lifetime of Thermally Fixed Holograms in $LiNbO_3$ Crystals Doped with Mg and Fe. *Appl. Phys. B* **2007**, *86*, 105–109.

36. Carrascosa, M.; Garcia-Cabanes, A.; Jubera, M.; Ramiro, J. B.; Agullo-Lopez, F. $LiNbO_3$: A Photovoltaic Substrate for Massive Parallel Manipulation and Patterning of Nano-Objects. *Appl. Phys. Rev.* **2015**, *2*.

37. Lucchetti, L.; Kushnir, K.; Reshetnyak, V.; Ciciulla, F.; Zaltron, A.; Sada, C.; Simoni, F. Light-Induced Electric Field Generated by Photovoltaic Substrates Investigated Through Liquid Crystal Reorientation. *Opt. Mater.* **2017**, *73*, 64 – 69.

38. Bhimanapati, G. R.; Lin, Z.; Meunier, V.; Jung, Y.; Cha, J.; Das, S.; Xiao, D.; Son, Y.; Strano, M. S.; Cooper, V. R.; Liang, L.; Louie, S. G.; Ringe, E.; Zhou, W.; Kim, S. S.; Naik, R. R.; Sumpter, B. G.; Terrones, H.; Xia, F.; Wang, Y. *et al.* Recent Advances in Two-Dimensional Materials beyond Graphene. *ACS Nano* **2015**, *9*, 11509–11539.

39. Liu, Y.; Weiss, N. O.; Duan, X.; Cheng, H.-C.; Huang, Y.; Duan, X. Van der Waals Heterostructures and Devices. *Nat. Rev. Mater.* **2016**, *1*.

40. Novoselov, K. S.; Mishchenko, A.; Carvalho, A.; Castro Neto, A. H. 2D Materials and Van der Waals Heterostructures. *Science* **2016**, *353*.

41. Manzeli, S.; Ovchinnikov, D.; Pasquier, D.; Yazyev, O. V.; Kis, A. 2D Transition Metal Dichalcogenides. *Nat. Rev. Mater.* **2017**, *2*.

42. Xia, F.; Perebeinos, V.; Lin, Y.-m.; Wu, Y.; Avouris, P. The Origins and Limits of Metal-Graphene Junction Resistance. *Nat. Nanotechnol.* **2011**, *6*, 179–184.

43. Venugopal, A.; Colombo, L.; Vogel, E. M. Contact Resistance in Few and Multilayer Graphene Devices. *Appl. Phys. Lett.* **2010**, *96*.

44. Smith, J. T.; Franklin, A. D.; Farmer, D. B.; Dimitrakopoulos, C. D. Reducing Contact Resistance in Graphene Devices through Contact Area Patterning. *ACS Nano* **2013**, *7*, 3661–3667.

45. Boggild, P.; Mackenzie, D. M. A.; Whelan, P. R.; Petersen, D. H.; Buron, J. D.; Zurutuza, A.; Gallop, J.; Hao, L.; Jepsen, P. U. Mapping the Electrical Properties of Large-Area Graphene. *2D Mater.* **2017**, *4*.

46. Chen, F. S. Optically Induced Change of Refractive Indices in $LiNbO_3$ and $LiTaO_3$. *J. Appl. Phys.* **1969**, *40*, 3389–3396.

47. Hsieh, H.; Psaltis, D.; Beyer, O.; Maxein, D.; von Korff Schmising, C.; Buse, K.; Sturman, B. Femtosecond Holography in Lithium Niobate Crystals. *Opt. Lett.* **2005**, *30*, 2233–2235.

48. Paipulas, D.; Buivydas, R.; Juodkazis, S.; Mizeikis, V. Local Photorefractive Modification in Lithium Niobate Using Ultrafast Direct Laser Write Technique. *J. Laser Micro/Nanoeng.* **2016**, *11*, 246–252.

49. Chan, J.; Venugopal, A.; Pirkle, A.; McDonnell, S.; Hinojos, D.; Magnuson, C. W.; Ruoff, R. S.; Colombo, L.; Wallace, R. M.; Vogel, E. M. Reducing Extrinsic Performance-Limiting Factors in Graphene Grown by Chemical Vapor Deposition. *ACS Nano* **2012**, *6*, 3224–3229.

50. Pirkle, A.; Chan, J.; Venugopal, A.; Hinojos, D.; Magnuson, C. W.; McDonnell, S.; Colombo, L.; Vogel, E. M.; Ruoff, R. S.; Wallace, R. M. The Effect of Chemical Residues on the Physical and Electrical Properties of Chemical Vapor Deposited Graphene Transferred to SiO_2. *Appl. Phys. Lett.* **2011**, *99*.

51. Thongrattanasiri, S.; Silveiro, I.; Javier Garcia de Abajo, F. Plasmons in Electrostatically Doped Graphene. *Appl. Phys. Lett.* **2012**, *100*.

52. Miro, P.; Audiffred, M.; Heine, T. An Atlas of Two-Dimensional Materials. *Chem. Soc. Rev.* **2014**, *43*, 6537–6554.

53. Mas-Balleste, R.; Gomez-Navarro, C.; Gomez-Herrero, J.; Zamora, F. 2D Materials: to Graphene and Beyond. *Nanoscale* **2011**, *3*, 20–30.

54. Ponraj, J. S.; Xu, Z.-Q.; Dhanabalan, S. C.; Mu, H.; Wang, Y.; Yuan, J.; Li, P.; Thakur, S.; Ashrafi, M.; Mccoubrey, K.; Zhang, Y.; Li, S.; Zhang, H.; Bao, Q. Photonics and Optoelectronics of Two-Dimensional Materials Beyond Graphene. *Nanatechnology* **2016**, *27*.

55. Mak, K. F.; Lee, C.; Hone, J.; Shan, J.; Heinz, T. F. Atomically Thin MoS_2: A New Direct-Gap Semiconductor. *Phys. Rev. Lett.* **2010**, *105*.

56. Vogt, P.; De Padova, P.; Quaresima, C.; Avila, J.; Frantzeskakis, E.; Asensio, M. C.; Resta, A.; Ealet, B.; Le Lay, G. Silicene: Compelling Experimental Evidence for Graphene like Two-Dimensional Silicon. *Phys. Rev. Lett.* **2012**, *108*.

57. Liu, H.; Neal, A. T.; Zhu, Z.; Luo, Z.; Xu, X.; Tomanek, D.; Ye, P. D. Phosphorene: An Unexplored 2D Semiconductor with a High Hole Mobility. *ACS Nano* **2014**, *8*, 4033–4041.

58. Ferrari, A. C.; Basko, D. M. Raman Spectroscopy as a Versatile Tool for Studying the Properties of Graphene. *Nat. Nanotechnol.* **2013**, *8*, 235–246.

Graphical TOC Entry